J. Geomag. Geoelectr., **40**, 1445–1467, 1988

A Separation of Ionospheric and Oceanic Tidal Components in Magnetic Fluctuation Data

N. L. BINDOFF[1]*, F. E. M. LILLEY[1], and J. H. FILLOUX[2]

[1]*Research School of Earth Sciences, The Australian National University, G.P.O. Box 4, Canberra, ACT 2601, Australia*
[2]*Scripps Institution of Oceanography, University of California at San Diego, La Jolla, California 92093, U.S.A.*

(Received January 5, 1988; Revised August 17, 1988)

Signals at tidal frequencies are observed in magnetic fluctuations recorded along a line of sites spanning the region from inland Australia to the floor of the central Tasman Sea. Assuming the site furthest inland to be free from oceanic tidal effects, the M_2 signal at 1.93 cycle·day^{-1} at each other site along the line is separated into a part due to a tidally-driven ionospheric dynamo, and a part due to a tidally-driven oceanic dynamo. Two factors are crucial to the separation method: the recognition that the ionospheric dynamo produces frequencies (known as the partial tides, and the phase-law tides), not associated with the oceanic dynamo; and the construction and use of an ionospheric induction transfer function, taken to be constant from continent to ocean.

The separations thus carried out show that for the deep-ocean sites in the Tasman Sea, the ionospheric dynamo and the oceanic dynamo make comparable contributions to the horizontal fluctuations observed at the frequency of the M_2 tide. The vertical fluctuation component at this frequency is almost entirely due to the oceanic dynamo. There is agreement with some features predicted by theoretical models.

1. Introduction

There are two principal sources of the signals at tidal frequencies which occur in observations of natural magnetic fields. The first source is the tidal motion in the Earth's upper atmosphere and ionosphere. The cause of this motion is the gravitational attraction of the Sun and the Moon, together with some solar heating. Winds thus generated in the electrically conductive ionosphere cut the flux lines of the Earth's steady magnetic field and generate electric currents, which act as primary source fields and induce secondary currents in the electrically conductive Earth. At the Earth's surface the primary and secondary fields are superimposed.

The second source of tidal signals is the tidal motion of the oceans, which is of gravitational origin only. The oceanic tidal currents also cause dynamo action by

*Now at Department of Earth, Atmospheric and Planetary Sciences, M.I.T., Cambridge, MA 02139, U.S.A.

their movement through the Earth's steady magnetic field. As a result, electric and magnetic fields are generated in the seawater, and couple (both Ohmically and inductively) with the conducting Earth.

Both sources of tidal signals are thus generated by dynamos. The ionospheric and oceanic dynamos have, however, different geometries and properties, and are located (respectively) external and internal to the "conductive" Earth. (In the context of this discussion, the conductive Earth is taken to include the oceans.) The separation of their contributions is important, both for the basic understanding of the dynamos, and for the use of the fields they generate to study electromagnetic induction in the Earth. One method of separation has been given by MALIN (1970, 1973), and see also SCHLAPP (1977) and WINCH (1981). The method of Malin is based on the assumption that the ionosphere has negligible electrical conductivity at local midnight, so that "geomagnetic tides" evident then are attributed in origin to the ocean. The method is essentially designed for application to data from a single observing station.

In the present paper, use is made of a linear array of stations, which span from inland Australia across a coastline to the floor of the central Tasman Sea. Certain lines of ionospheric origin in a tidal spectrum are identified by their "partial tide" or "phase-law tide" nature. At an inland site a transfer function is determined, which links a signal of definite ionospheric origin to a more general tidal line. Remote from the ocean, the general tidal line is also taken to be entirely of ionospheric origin.

This transfer function is then taken to hold at other sites along the linear array, including those sites which cross the coast, and those on the deep-sea floor. Thus an estimate of the ionospheric tide contribution is made for the seafloor data, and so an ionospheric-oceanic separation is carried out.

2. Experiment and Data

The data of the present paper are from the Tasman Project of Seafloor Magnetotelluric Exploration or Tasman experiment, which observed in 1983/84. The observation sites are shown in Fig. 1, and details of the experiment are given in FERGUSON (1988), BINDOFF (1988) and LILLEY *et al.* (1988). The seafloor instruments contributing data to the present paper were Filloux magnetometers (FILLOUX, 1987). The land instruments were Gough-Reitzel magnetometers (GOUGH and REITZEL, 1967; LILLEY *et al.*, 1975) and the Canberra Magnetic Observatory. Examples of the data recorded are given in Fig. 2. The season of the observations was the southern summer from early December 1983 to late March 1984.

Some basic notations adopted in this paper are H, D and Z for the components of magnetic fluctuation in the horizontal north, east and vertically downwards directions. The full length of a time series will be denoted by T. Time variation is generally taken to be according to $e^{-i\omega t}$, where ω is angular frequency. Phases given are thus generally phase lags, in the sense that a more positive phase shifts the signal to a later real time.

Individual tidal constituents will be described in this paper by their traditional

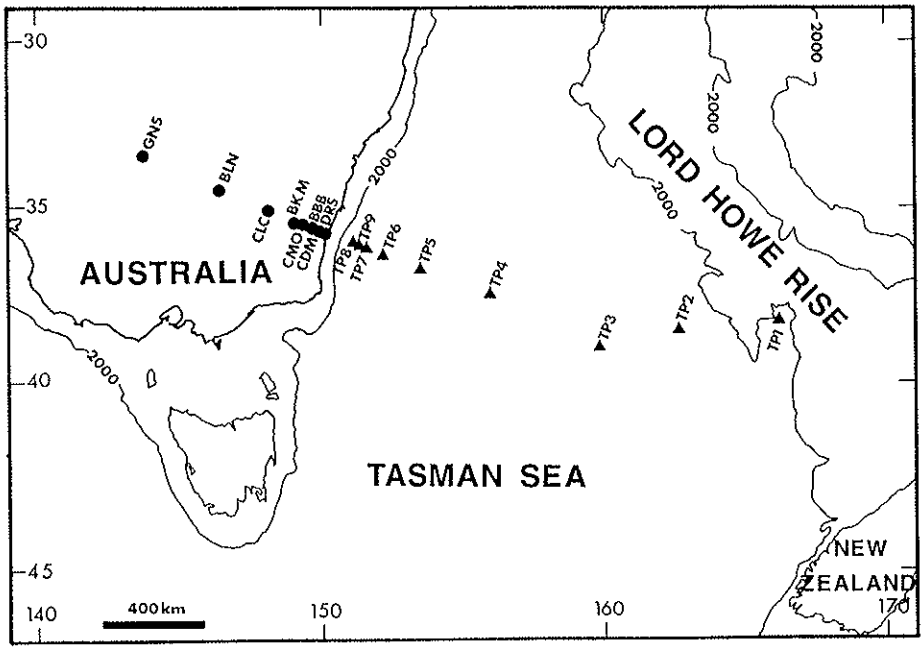

Fig. 1. Map of the observing sites for the Tasman experiment relevant to the present paper.

notation, for example M_2. The family of magnetic partial tides and phase-law tides (introduced in Section 3 below) which is driven by M_2 will collectively be denoted by $L(M_2)$, and an individual member of the family (of frequency ν_n) will be denoted $L(M_2, \nu_n)$. The paper involves analysis for signals at the expected tidal frequencies. The term "tidal line" will be used to mean a signal at a particular tidal frequency, rather than implying that in a spectrum of the experimental data the signal would appear as an ideal discrete "line".

3. Tidal Frequencies

3.1 The basic tides

The frequencies of the tides to be expected in the Earth's oceans and ionosphere come from the time dependence of the gravitational potentials of the Sun and Moon for an Earth-based observer, and are well-known (DOODSON and WARBURG, 1941; MELCHIOR, 1983). Due to the controlling influence of the Earth's rotation the main tides divide into two frequency bands, named diurnal and semi-diurnal. Table 1 lists the strongest tides of each band and gives their generally accepted code names. Table 1 also gives their expected relative sizes, scaled according to their known tide-generating potentials and taken relative to unity for the dominant tide in each band. The three strongest expected diurnal tides are K_1, O_1 and P_1, and the three strongest semi-diurnal tides are M_2, S_2 and N_2.

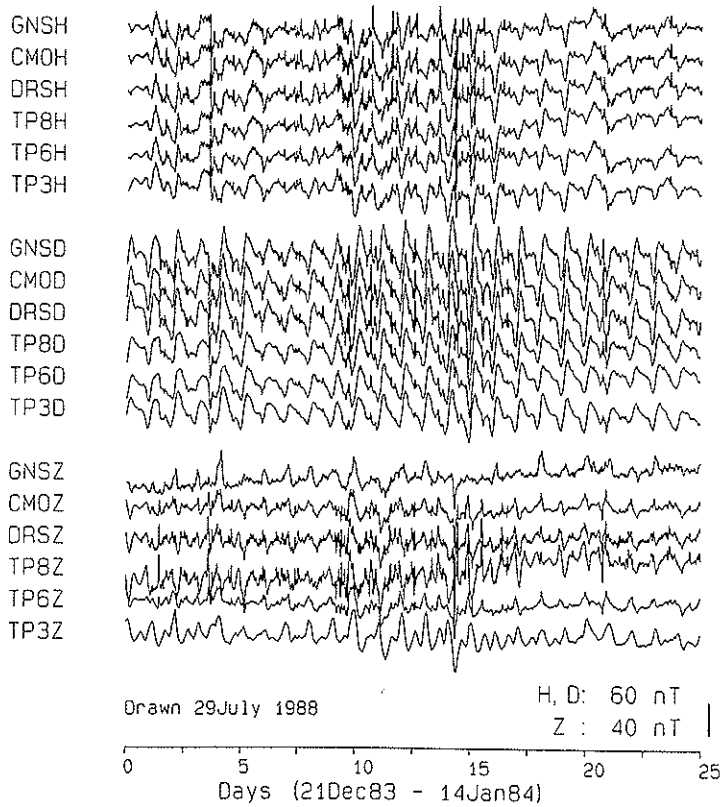

Fig. 2. Example (covering six sites and 25 days) of the magnetic fluctuation data set of the Tasman experiment. The code GNSH, for example, marks the H component recorded at site GNS.

In addition to the gravitational forces driving the tides, in the ionosphere there occur thermally-driven winds due to solar heating. These winds contribute significantly to the ionospheric dynamo at the periods of the harmonics of a mean solar day; that is, at frequencies denoted S_1, S_2, S_3 and S_4.

3.2 *Phase-law and partial tides*

The ionosphere, due to the influence of the Sun and relative to an Earth-based observer, has an electrical conductivity which varies periodically, though non-linearly with time (see for example MATSUSHITA, 1967 and VOLLAND, 1984). This phenomenon therefore causes a modulation of the electric currents, and, in turn, of the magnetic fluctuations which are generated in the ionosphere by tides and thermal winds. The temporally non-linear ionospheric ionisation and ion recombination responses to solar irradiation result in further strengthening of the solar harmonics S_2, S_3, etc. This modulation has the important effect of introducing extra

Table 1. The eleven strongest constituents in each of the diurnal and semi-diurnal tidal bands, with Darwinian notation, period, scaled size, and $\Delta\omega$ parameter (in cycle·day^{-1}).

Tidal Constituents

Diurnal constituent	Period (hours)	Frequency (cpd)	Proportion of largest	$\Delta\omega$ (cpd)
Q_1	26.868357	0.893244	0.136	0.106756
O_1	25.819341	0.929536	0.710	0.070464
M_1	24.833248	0.966446	0.040	0.033863
Π_1	24.132140	0.994524	0.020	0.005476
P_1	24.065890	0.997262	0.330	0.002738
S_1	24.000000	1.000000	0.008	0.000000
K_1	23.934469	1.002738	1.000	−0.002738
ψ_1	23.869299	1.005476	0.008	−0.005476
ϕ_1	23.804476	1.008214	0.014	−0.008213
J_1	23.098476	1.039030	0.056	−0.039030
OO_1	22.306074	1.075940	0.030	−0.075940

Semi-diu constituent	Period (hours)	Frequency (cpd)	Proportion of largest	$\Delta\omega$ (cpd)
$2N_2$	12.905374	1.859690	0.025	0.140310
μ_2	12.871757	1.864547	0.031	0.135453
N_2	12.658348	1.895982	0.192	0.104018
ν_2	12.626004	1.900839	0.036	0.099161
M_2	12.420601	1.932274	1.000	0.067726
λ_2	12.221774	1.963708	0.007	0.036292
L_2	12.191620	1.968565	0.028	0.031434
T_2	12.016449	1.997262	0.027	0.002738
S_2	12.000000	2.000000	0.467	−0.000000
R_2	11.983595	2.002738	0.004	−0.002738
K_2	11.967235	2.005476	0.127	−0.005476

frequencies associated with each tide-generating potential into the spectrum of tidal lines.

The time-dependence of the ionospheric electrical conductivity $\sigma(t)$ due to the influence of the sun may be expressed as a series such as

$$\sigma(t) = \sum_{n=0}^{k} \sigma_n \cos(2\pi n t - \phi_n) \qquad (1)$$

(see for example MALIN, 1973 and WINCH, 1981), where t denotes Universal time in mean solar days, and σ_n and ϕ_n denote amplitude and phase of an harmonic of the daily conductivity variation. (In principle, the seasonal modulation of the ionospheric conductivity has a further complicating effect, but such seasonal effects will be neglected here, due to the limited time duration of the Tasman experiment observations.) Thus each gravitational tide has associated with it a set of extra

magnetic tidal lines, $(2k-1)$ in number. Following WINCH and CUNNINGHAM (1972) each extra tide may be expressed (where X is the code for the "driving" tide)

$$L(X, \nu_n) = c_n \cos[2\pi\nu_n t - \varepsilon_n], \tag{2}$$

where c_n denotes amplitude, and ε_n denotes phase. The frequency in cycle·day^{-1} is given by ν_n

$$\nu_n = n - \Delta\omega,$$

where $\Delta\omega$ is set by the driving tide, and appropriate values (calculated from WINCH and CUNNINGHAM, 1972) are given in Table 1. The integer n lies in the range $(l-k)$ to $(l+k)$, where l has values of one or two according to whether the driving tide is diurnal or semi-diurnal. Thus the extra magnetic tidal lines of a particular family taken together may be expressed as

$$L(X) = \sum_{n=l-k}^{l+k} c_n \cos[2\pi\nu_n t - \varepsilon_n]. \tag{3}$$

In Eq. (2), when the frequency ν_n has a negative value, the signals should be observed as 180° out-of-phase with a signal of frequency $-\nu_n$.

Positive and negative values for n in Eq. (3) give rise to tides referred to as "phase-law tides" ($n>0$) and "partial tides" ($n\leq 0$) respectively. The range taken by n shows that for $k=4$ (commonly taken to be well adequate for Eq. (1)) each basic tide generates nine "phase-law" and "partial" tides. The twenty-two tides in Table 1 would thus generate a possible 198 spectral lines.

3.3 Practical considerations for the Tasman data

The Tasman experiment data, which consist of time series 60 to 120 days long, may not be expected to resolve all the spectral lines just described. Examination of the line separation in frequency space, and of the relative line sizes, shows that spectral analysis of the data is reasonably carried out on just 13 lines. The time series are approximately 100 days long and therefore have a maximum theoretical resolution of 0.01 cycle·day^{-1}.

Referring to the strong diurnal tides in Table 1, both K_1 and P_1 differ from S_1 by only 1 cycle·year^{-1}, and so all three will appear as a single line. The O_1 tide, however, should be resolved, as it differs from S_1 by 0.0704 cycle·day^{-1}. For the strong semi-diurnal tides, K_2 differs from S_2 by only 2 cycle·year^{-1} and so should not be resolved from it, whereas M_2 differs from S_2 by 0.0677 cycle·day^{-1} (six times the theoretical maximum resolution) and so should be a distinct line.

Thus, in the Tasman data, the strongest diurnal and semi-diurnal tides which should be resolved separately from the harmonics of a mean solar day are the O_1 and M_2 constituents, respectively. Due to the daily variation of the ionospheric electrical conductivity these two constituents will generate multiple tidal lines in an observed

magnetic spectrum, of frequencies (according to Subsection 3.2 and taking $k=4$) given by

$$(n - \Delta\omega_{O_1}) \quad \text{with } n = -3, -2, \ldots, 0, \ldots, 4, 5 \text{ for } O_1,$$

and

$$(n - \Delta\omega_{M_2}) \quad \text{with } n = -2, -1, 0, \ldots, 5, 6 \text{ for } M_2,$$

where $\Delta\omega_{O_1}$ and $\Delta\omega_{M_2}$ refer to the $\Delta\omega$ values in Table 1 for O_1 and M_2.

It is now relevant to note that pairs of these families of lines are close together in frequency, and so may be expected to be indistinguishable in the Tasman experiment data. For example, for $n=2$ and $\Delta\omega_{O_1}=+0.070464$

$$(n - \Delta\omega_{O_1}) = 1.929536 \text{ cycle}\cdot\text{day}^{-1},$$

whereas for $n=2$ and $\Delta\omega_{M_2}=+0.067726$

$$(n - \Delta\omega_{M_2}) = 1.932274 \text{ cycle}\cdot\text{day}^{-1}.$$

Thus, the additional magnetic tides given by Eq. (3) for the O_1 and M_2 constituents cannot be separated in the present data on the basis of frequency alone. A similar situation also arises for the Q_1 and N_2 families of lines generated by Eq. (3), which form pairs the individual members of which again differ from each other by only 1 cycle·year^{-1}.

The dominant lines in a "magnetic tide" spectrum of Tasman experiment data may thus be expected to be at frequencies described by the harmonics of a mean solar day (S_1, S_2, S_3, S_4), and the $L(M_2)$ and $L(N_2)$ families of magnetic tides. The analysis to follow will thus concentrate on signals at these frequencies. For the reasons given, each spectral line found in the data may represent the combined effect of several different physical causes. Thus in the remainder of this paper tide code-names are used to identify frequency, rather than to imply the origin or source of a particular signal. For example, the family of lines denoted $L(M_2)$ will now in principle include the effects of both the basic M_2 and O_1 tides, of both oceanic and ionospheric origin, together with all extra magnetic tides generated by the M_2 and O_1 driving tides according to Eq. (3).

4. Observed Tides

4.1 Fourier spectra

Basic Fourier analysis of examples of the recorded time series illustrates some of the points just discussed. Figure 3 ((a) and (b)) presents Fourier series amplitudes for the H-component fluctuation records for the inland site GNS, and the deep-ocean seafloor site TP3 (both sites are shown on Fig. 1). The full lengths of the time

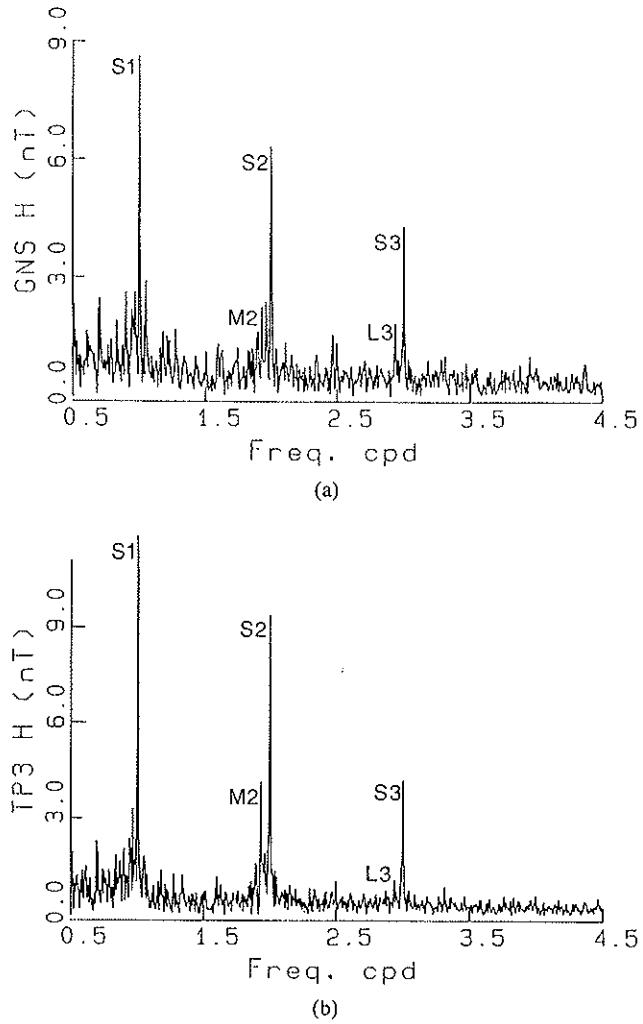

Fig. 3. (a) Plot of Fourier coefficients for the H component record at the inland site GNS. (b) Plot of Fourier coefficients for the H component record at the seafloor site TP3.

series (121 days for GNS and 111 days for TP3) have been analyzed taking 15-minute means of the original time series (but without other filtering or smoothing) to give the coefficient amplitudes shown.

The spectrum for GNS (Fig. 3(a)) shows lines at the S_1, S_2 and S_3 frequencies, and two lines from the $L(M_2)$ family at 1.93 cycle·day^{-1} and 2.93 cycle·day^{-1} (marked M_2 and L_3). The spectrum for TP3 in Fig. 3(b) shows the same peaks, and in addition a weak N_2 line at 1.89 cycle·day^{-1} from the $L(N_2)$ family.

4.2 Least-squares techniques

Using the Fourier coefficient spectra of Fig. 3 as a guide to the discrete lines present in the observed data, more accurate estimates of the tidal signals have been made using least-squares methods to fit lines of specified frequency. For the reasons discussed in Subsection 3.3, the specified frequencies comprise three categories

(i) the S_1, S_2, S_3 and S_4 harmonics of the solar day;

(ii) eight members of the $L(M_2)$ family; and

(iii) the N_2 frequency.

The single N_2 line was included because of its evidence in Fig. 3(b).

Details of the numerical techniques adopted are given in Appendix 1. The results of the least-squares analysis and statistical tests are given in Table 2, for all three magnetic components recorded at both sites GNS and TP3. Some observations about the results of Table 2 are as follows:

(i) Of the thirteen frequencies fitted to the time series, some are consistently insignificant at the 90% level, and so (in hindsight) need not have been included in the analysis.

(ii) The three harmonics S_1, S_2 and S_3 are all significant in excess of the 99% level, for all components, at both sites.

(iii) The relatively low values of the F-statistic for the S_2 lines, compared to its values for the S_1 and S_3 lines, implies that the background noise level around this frequency (of 2 cycle·day^{-1}) is relatively high. This level of noise may be a result of other signals of ionospheric or magnetospheric origin, or seasonal effects in ionospheric conductivity not associated with the S_1 and S_3 harmonics.

(iv) The horizontal components H and D have a different behaviour from the Z component. The H component shows the presence of two lines from the $L(M_2)$ family which are significant at the 99% level; these lines are at 1.93 and 2.93 cycle·day^{-1}. The D component has three lines significant at the 99% level from $L(M_2)$ group; two lines as for H plus 0.93 cycle·day^{-1}.

4.3 Criterion for an M_2 ionospheric dynamo

The conductivity of the deep ocean does not have a daily variation in electrical conductivity similar to that of the ionosphere given in Eq. (1), and therefore the tides of the ocean cannot directly generate the additional "phase-law" and "partial" spectral lines of Eq. (3). Thus the presence of the spectral line at 2.93 cycle·day^{-1} observed in the H and D records at both the inland site GNS and the seafloor site TP3 establishes that an M_2 tidally-driven ionospheric dynamo is present during the recording period. This observation necessarily implies that the spectral lines at the M_2 driving frequency of 1.93 cycle·day^{-1} for the ocean sites of the Tasman experiment must contain some contributions of ionospheric origin, in addition to their expected contributions of oceanic origin.

4.4 Analysis of other driving forces

In the H component analysis, the 0.93 cycle·day^{-1} line is not significant at the 90% level, indicating the absence of an O_1 driving tide. Thus, for the H component,

Table 2. Results in terms of amplitude and phase values for the least-squares fitting of thirteen specified tides to the H (Table 2(a)), D (Table 2(b)) and Z (Table 2(c)) data from sites GNS and TP3. The statistical F-values are derived as given in Appendix 1, and a cross is marked in the Tables where a tidal line is significant at the 90, 95 or 99% confidence level.

(a)

			GNS: Land magnetometer						TP3: Seafloor Magnetometer					
Comp.	Name phase	Frequency (cpd)	F-value	Confidence level 90%	95%	99%	Amp. (nT)	Phase (deg)	F-value	Confidence level 90%	95%	99%	Amp. (nT)	Phase (deg)
H	S_1	1.00000	162.9	×	×	×	7.4	−165.8	667.4	×	×	×	12.9	178.4
	S_2	2.00000	10.9	×	×	×	6.3	−166.5	11.7	×	×	×	9.7	−173.6
	S_3	3.00000	199.8	×	×	×	4.0	−140.8	236.4	×	×	×	4.0	−160.9
	S_4	4.00000	0.1				0.4	−75.1	0.0				0.4	128.7
	N_2	1.89598	1.4				0.8	21.5	4.3	×	×		1.7	46.4
	$L(M_2)$	−2.06773	0.2				0.3	146.8	0.0				0.1	113.0
		−1.06773	4.4	×	×		1.2	83.6	3.6	×	×		0.9	104.8
		−0.06773	143.2				0.0	−27.8	101.4				0.0	150.8
		0.93233	1.5				0.7	96.6	1.2				0.5	115.7
		1.93233	11.7	×	×	×	2.0	74.9	22.7	×	×	×	4.6	63.3
		2.93233	50.7	×	×	×	1.6	86.1	35.9	×	×	×	1.2	70.5
		3.93233	0.8				0.5	125.3	0.2				0.2	83.4
		4.93233	1.1				0.3	42.5	0.8				0.2	55.3

(b)

Comp.	Name phase	Frequency (cpd)	GNS: Land magnetometer						TP3: Seafloor Magnetometer					
			F-value	Confidence level 90%	95%	99%	Amp. (nT)	Phase (deg)	*F*-value	Confidence level 90%	95%	99%	Amp. (nT)	Phase (deg)
D	S_1	1.00000	3189.3	×	×	×	20.8	107.0	4395.7	×	×	×	19.7	104.4
	S_2	2.00000	283.7	×	×	×	17.4	156.1	120.6	×	×	×	11.1	155.0
	S_3	3.00000	422.6	×	×	×	7.6	172.9	139.8	×	×	×	3.8	157.4
	S_4	4.00000	0.1				0.9	−167.6	0.1				0.6	154.1
	N_2	1.89598	3.3	×			1.2	29.6	2.1				0.7	3.3
	$L(M_2)$	−2.06773	2.8				1.2	151.1	1.0				0.9	113.6
		−1.06773	0.5				0.3	97.0	2.4				0.4	−43.4
		−0.06773	4.2				0.0	−46.5	1.6				0.0	−92.8
		1.93233	17.2	×	×	×	1.7	−49.2	12.4	×	×	×	1.5	−39.3
		1.93233	17.7	×	×	×	3.4	20.0	14.0	×	×	×	3.3	6.3
		2.93233	30.7	×	×	×	1.5	24.0	7.9	×	×	×	0.7	3.6
		3.93233	0.5				0.7	62.9	0.1				0.1	53.4
		4.93233	3.6	×	×		0.4	−24.0	3.1	×			0.2	19.3

(c)

Comp.	Name phase	Frequency (cpd)	GNS: Land magnetometer						TP3: Seafloor Magnetometer					
			F-value	Confidence level 90%	95%	99%	Amp. (nT)	Phase (deg)	*F*-value	Confidence level 90%	95%	99%	Amp. (nT)	Phase (deg)
Z	S_1	1.00000	565.0	×	×	×	5.8	18.2	910.8	×	×	×	7.8	5.1
	S_2	2.00000	12.6	×	×	×	4.3	80.7	14.9	×	×	×	6.7	90.5
	S_3	3.00000	166.4	×	×	×	2.2	114.2	167.6	×	×	×	2.2	108.0
	S_4	4.00000	0.6				0.3	169.2	0.2				0.2	135.7
	N_2	1.89598	1.8				0.4	29.7	10.8	×	×	×	1.2	30.1
	$L(M_2)$	−2.06773	0.2				0.2	−59.6	0.5				0.2	−178.3
		−1.06773	15.8	×	×	×	0.8	10.7	4.4	×	×		0.6	4.5
		−0.06773	8.6				0.0	132.1	0.4				0.0	26.1
		0.93233	1.2				0.2	−178.1	6.0	×	×	×	0.5	−78.8
		1.93233	2.0				0.6	−24.9	84.1	×	×	×	4.6	−14.4
		2.93233	5.1	×	×		0.4	16.1	0.6				0.1	−49.0
		3.93233	0.1				0.1	4.9	0.0				0.1	−48.9
		4.93233	0.6				0.1	63.5	1.2				0.1	−43.5

the $L(M_2)$ lines may be driven by the M_2 tide only. The D component analyses however show the 0.93 cycle·day^{-1} line to be significant at the 99% level at both sites, allowing the O_1 tide, in addition to the M_2 tide, to be driving the $L(M_2)$ family of magnetic tides for D.

For the Z components, the results in Table 2 depend on the location of the site. For the inland site GNS, the most significant (at the 99% level) of the $L(M_2)$ family of lines is -1.06 cycle·day^{-1}, with 2.93 cycle·day^{-1} significant at the 95% level. The basic M_2 frequency of 1.93 cycle·day^{-1} is not significant, so that it appears the M_2 ionospheric dynamo generates only small and not significant lines in Z.

At the seafloor site, TP3, the ionospherically driven magnetic tidal lines are statistically less significant than at the land site GNS. However, the 0.93 and 1.93 cycle·day^{-1} lines (corresponding to the O_1 and M_2 basic tides) are both significant to the 99% level; the absence of other magnetic tides indicates that these lines are indeed due to the direct action of O_1 and M_2 oceanic tides.

5. Separation of Source Fields

(In this section, the shortened notation will be used of L_2 and L_3 for $L(M_2, 2-\Delta\omega_{M_2})$ and $L(M_2, 3-\Delta\omega_{M_2})$ respectively. The notations ${}^{A}L_2$ and ${}^{A}L_3$ will mean L_2 and L_3 observed at site A.)

The evidence discussed in Section 4 established the presence of both ionospheric and oceanic tidal source-effects in the seafloor magnetic variation data. A method for separating these two effects in the L_2 spectral line is now developed, based on analysis of data from the inland station GNS. Due to its distance inland from the sea (640 km from the east Australian coastline), station GNS is assumed to be free of oceanic tidal effects, an assumption supported by the tidal models of LARSEN (1968), HEWSON-BROWNE (1973) and CHAVE (1983) which show that the magnetic field signals due to the ocean tides are either small or decay rapidly with distance inland from the ocean edge (or both).

Then at any general station A consider the observed M_2 tidal line ${}^{A}L_2$ to be composed of a part of ionospheric dynamo origin ${}^{A}L_2^{I}$ and a part of oceanic dynamo origin ${}^{A}L_2^{O}$. Thus

$$ {}^{A}L_2 = {}^{A}L_2^{I} + {}^{A}L_2^{O}, $$

or

$$ {}^{A}L_2^{O} = {}^{A}L_2 - {}^{A}L_2^{I}. \tag{4} $$

The ${}^{A}L_3$ line will comprise a part of ionospheric dynamo origin only, so that

$$ {}^{A}L_3 = {}^{A}L_3^{I} $$

and

$$^{A}L_3^{O} = 0.$$

At station GNS, due to distance from the ocean,

$$^{GNS}L_2^{O} = 0$$

and

$$^{GNS}L_2^{I} = {}^{GNS}L_2.$$

Nearer the coast or on the seafloor, at a general station A, $^{A}L_2^{O}$ cannot be assumed to be zero, but a zero-th order approximation could be based on taking

$$^{A}L_2^{I} = {}^{GNS}L_2^{I}. \tag{5}$$

Implicit in Eq. (5) is the assumption that neither the driving source field nor the general electrical conductivity structure vary spatially from station A to station GNS. For such a restricted case

$$^{A}L_2^{O} = {}^{A}L_2 - {}^{GNS}L_2,$$

and the magnetic field components of ionospheric and oceanic origin may be separated.

In practice, however, the electrical conductivity structure will change between two such stations, reducing the validity of Eq. (5). This difficulty may be overcome partly if the induction scales are comparable for L_2^{I} and L_3^{I}. Then the ionospheric contribution $^{A}L_2^{I}$ may be estimated as

$$^{A}L_2^{I} = \frac{^{GNS}L_2^{I}}{^{GNS}L_3} \cdot {}^{A}L_3, \tag{6}$$

an approximation which in turn depends on the ratio of L_2^{I} and L_3^{I} remaining constant from inland to coastal or seafloor sites.

Defining a transfer function T as the quantity

$$T = \frac{^{GNS}L_2^{I}}{^{GNS}L_3} = \frac{^{GNS}L_2}{^{GNS}L_3}, \tag{7}$$

a separation of the oceanic and ionospheric parts is achieved by combining (4), (6) and (7) to obtain

$$^{A}L_2^{I} = T \cdot {}^{A}L_3 \tag{8}$$

and

$$^{A}L_2^{O} = {}^{A}L_2 - T \cdot {}^{A}L_3. \tag{9}$$

Thus the separation relies on determining the transfer function T at the inland station GNS, on observations of $^{A}L_2$ and $^{A}L_3$ at station A, and on the assumption that $^{A}L_3^{O}=0$, which is easily satisfied since the M_3 tide is negligibly small.

Before applying Eq. (9) to the observed data a theoretical phase correction to the transfer function T is possible, and indeed desirable in a case like the Tasman experiment where the observing line extends some 2000 km in an east-west direction.

The phase correction is based on the L_2 and L_3 source fields having different horizontal wavelengths, taken to be 180° and 120° of longitude, and corresponding to phase variations at a fixed observing site of 30° hour^{-1} and 45° hour^{-1} respectively. Thus the phase of T should increase by 1° per increasing degree of longitude eastward. With such a phase correction to T, Equation (8) becomes

$$^{A}L_2^{I} = e^{i\lambda} T \cdot {}^{A}L_3, \tag{10}$$

and Equation (9) becomes

$$^{A}L_2^{O} = {}^{A}L_2 - e^{i\lambda} T \cdot {}^{A}L_3, \tag{11}$$

where site A is λ degrees of longitude east of site GNS.

The main advantage of the transfer function T in the separation of oceanic and ionospheric contributions (as defined in Eq. (7)) is that it should be insensitive to differences in conductivity structure between the reference site and other land and seafloor sites. This point is first demonstrated by considering the ideal case in which the induction scales of L_2^{I} and L_3^{I} are the same, and their respective source currents have the same configuration. In such a case, due to the linearity of Maxwell's equations, the induced electric and magnetic fields associated with L_2^{I} and L_3^{I} will occur in the same relative proportions at each site. Consequently, the transfer function T will be an invariant function of space.

However, in practice for the Earth the induction scales of the L_2^{I} and L_3^{I} geomagnetic tides will differ, and the transfer function will have some dependence on electrical conductivity structure. The most significant electrical conductivity difference between the reference site and the seafloor sites is that of the ocean. Calculations of the relative attenuation of L_2^{I} and L_3^{I} for a one-dimensional model, using the sub-oceanic conductivity structure of FILLOUX (1980), show that the amplitude of the transfer function T at the seafloor is increased by a factor of 1.2 over the sea-surface value. This result implies that at seafloor sites, the ionospheric component L_2^{I} is systematically underestimated by the transfer function method adopted here.

The effects of horizontal conductivity variations are more difficult to assess. However, using similar ionospheric transfer functions applied to the second and third harmonics of the daily variation BINDOFF (1988) concludes that the horizontal

magnetic fluctuation components, at seafloor sites, are underestimated in amplitude by a factor of 1.1 to 1.4 (depending on the component). This result is accounted for by the different attenuations of the harmonics through the ocean water, and it is expected in the present paper also that the main source of systematic error will be from this cause, rather than from variation in deeper electrical conductivity structure.

In the next section, separations will be presented which have been carried out by the application of Eq. (11) to the line of stations of the Tasman experiment. Three transfer functions have first been determined for the H, D and Z components at station GNS, by substituting the appropriate values from Table 2 into Eq. (7). The values obtained for the transfer functions are given in Table 3.

6. Results

Using the technique described in the previous section, the L_2 spectral line has been separated into parts of ionospheric and oceanic origin, for each of the three magnetic field components at all sites (except CMO and BBB) shown in Fig. 1. The results for each of the magnetic field components are shown in Figs. 4(a), (b) and (c). The error bars on the amplitude terms have been calculated from the formulae given by BRILLINGER (1981, p. 188), using estimates of the standard deviation for each of the quantities L_2^I and L_2^O. The standard deviations on L_2^I and L_2^O were found by the simple algebraic rules for combining errors, using estimates of the standard deviation on the least-squares fitted line L_2, and on the transfer function given in Table 3. The error bars shown in Figs. 4(a), (b) and (c) are for one standard deviation, and using F tables the amplitude error bar may be converted to a 95% confidence interval for 2 over ∞ degrees of freedom by multiplying by the factor 2.449.

The main contribution to the size of the error bars on either the L_2^O or the L_2^I spectral lines is the large relative error associated with the transfer function, calculated from the reference site GNS. Depending on the component, the standard deviation is 24% to 45% of the transfer function (see Table 3). This large error is due to the intrinsic noise from non-deterministic processes always present in magnetic variation data. The spectra shown in Figs. 2(a) and (b) give an indication of the background noise level around each of the spectral lines fitted to the time series.

Table 3. Transfer functions determined for site GNS, with estimates of standard deviation.

	Comp.	Transfer function		Standard deviation	
		Amp. (nT)	Phase (deg)	Amp. (nT)	Phase (deg)
GNS	H	1.238	−11.2	0.333	8.4
	D	2.286	−3.9	0.555	14.1
	Z	1.468	−41.4	0.657	26.6

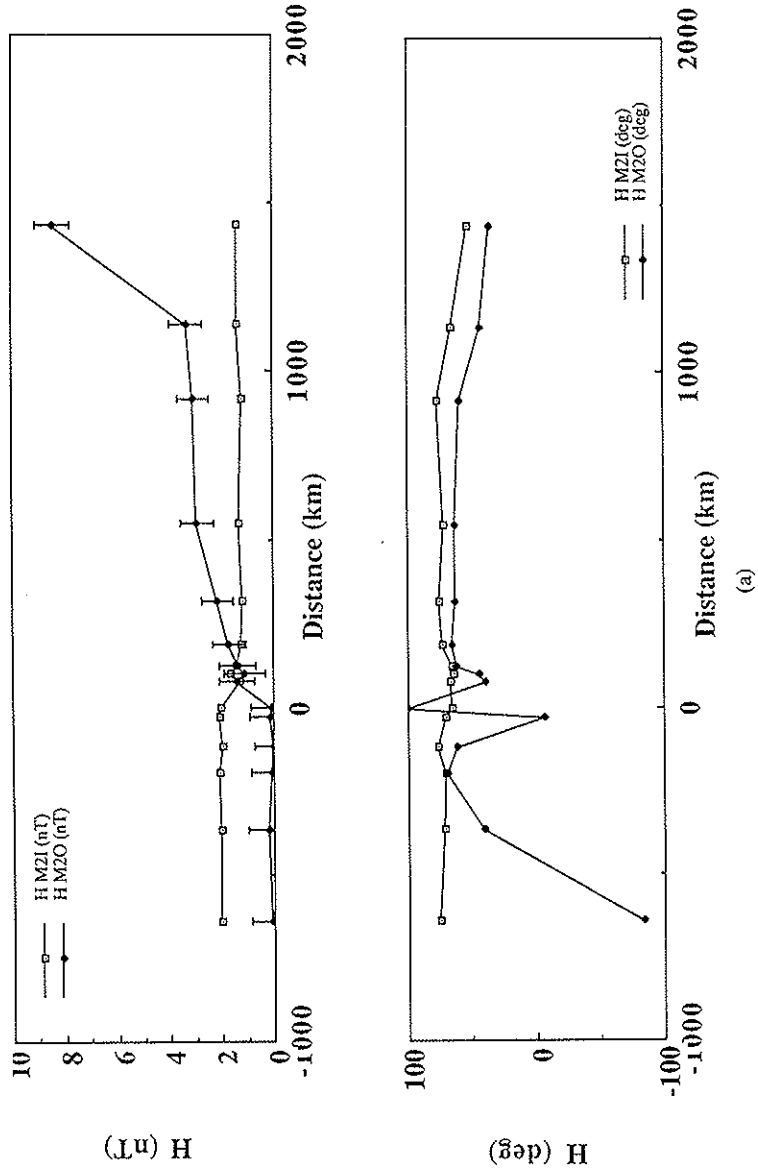
H M2I (nT)
H M2O (nT)
H (nT)
10
8
6
4
2
0
-1000
0
1000
2000
Distance (km)
H M2I (deg)
H M2O (deg)
H (deg)
100
0
-100
-1000
0
1000
2000
Distance (km)

(a)

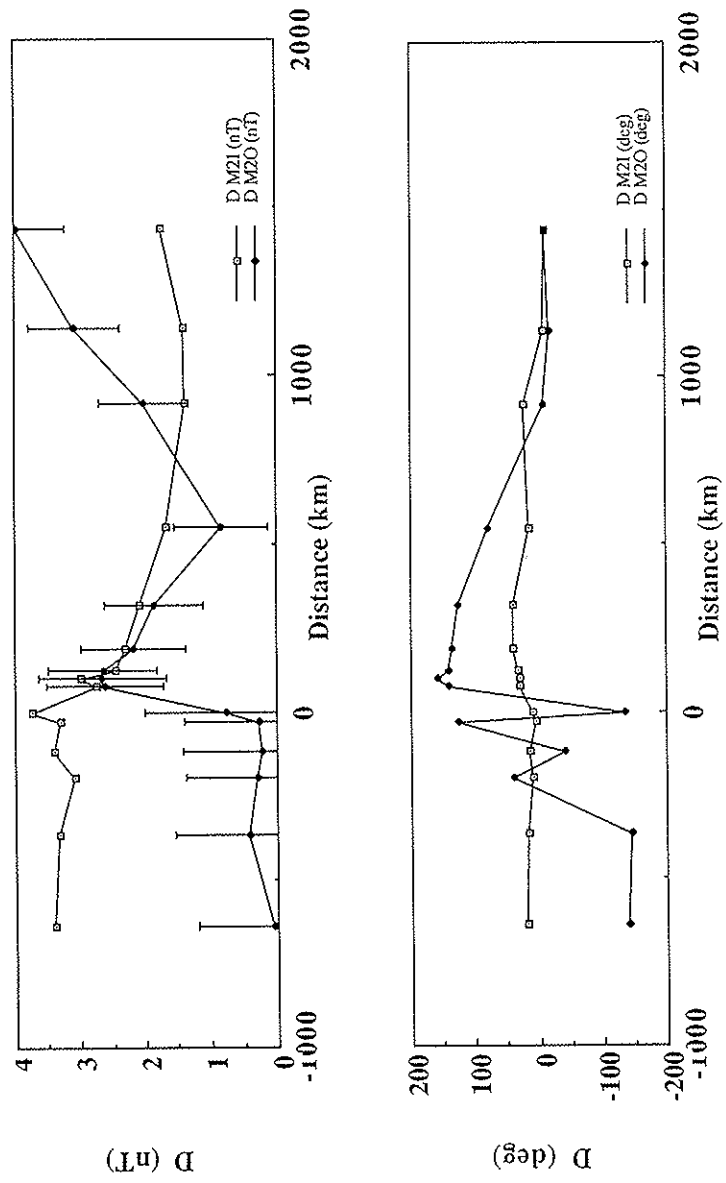

Fig. 4. Separation of magnetic fluctuations at the M_2 tidal frequency into parts of ionospheric-dynamo and oceanic-dynamo origin, at all stations (except CMO and BBB) along the line of the Tasman experiment (see Fig. 1). The zero for distance measurement is the coastal site DRS, and distance along the Tasman observing line increases positive eastwards. Amplitude values (in nT) and phase values (in degrees) are shown in separate graphs for the separated parts. (a) Separation for the H component. The part of ionospheric-dynamo origin is HM2I, and that of oceanic-dynamo origin is HM2O, in the figure legend. (b) Separation for the D component. (c) Separation for the Z component.

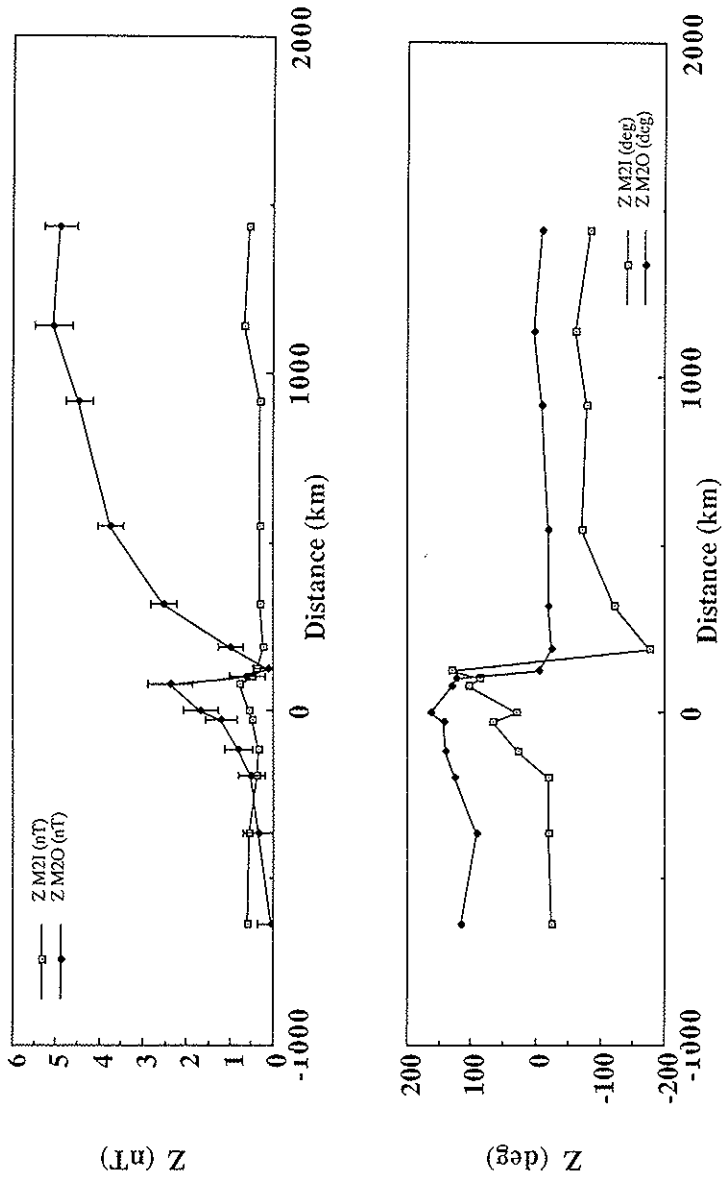

(c)

Fig. 4. (continued).

Figures 4(a), (b) and (c) show that the separations of sources of ionospheric and oceanic origin exhibit systematic behaviour across the Tasman experiment profile. Inland, the site-to-site variations for the ionospheric and oceanic source fields are small. These two features, taken together, suggest strongly that the separation of the L_2 spectral line into parts of oceanic and ionospheric origin is a stable and well-behaved process.

Also in Fig. 4, the separated ionospheric contributions to the horizontal components H and D (Z is barely resolved) show that the source field is moving from east to west. The phase velocity of the external source, based on the difference in phase between the two ends of the array, is 14.7° hour^{-1} and 19.6° hour^{-1} for H and D respectively. Given the uncertainty in the phase estimation, these phase velocities are consistent with the phase velocity of the ionospheric driving potential, and reflect the large-scale size of the external inducing field. On the ocean side of the ocean-continent boundary, the ionospheric contribution of the D component phase is later than expected from the source velocity; this result resembles the "sticking" effect described by RODEN (1964) and BULLARD and PARKER (1971) for an east-west moving source-field over a conductive region. The step-like jumps in the amplitudes of the D and H components across the ocean-continent boundary, of 2 nT and 0.8 nT respectively, are due to the seafloor instruments being situated below the electric currents induced in the ocean.

The oceanic contributions shown in Figs. 4(a), (b) and (c) have a different character to the ionospheric contributions. The horizontal components of L_2^O at the inland sites are statistically insignificant, with phase values unresolved. In contrast, the amplitude of the inland vertical component is statistically significant at the near-coastal sites and increases smoothly towards the coast from reference site GNS, to reach a local maximum just offshore at site TP8. These characteristics of the horizontal and vertical components of the oceanic contribution to L_2 are consistent with a source of electric currents confined to the Tasman Sea.

The D and H oceanic components are significant at all seafloor sites. The phase of the D component varies by 152° over the seafloor portion of the array, a distance of just less than 1500 km. This large phase change is indicative of the relatively short scale-size of the electric current generated by the M_2 ocean tides, which are constrained to flow in the Tasman Sea. The phase of the H component varies by 29°, indicating that the east-west electric currents do not reverse their direction over the seafloor array. The general form of the separated oceanic magnetic field components in Figs. 4(a), (b) and (c) appears consistent with electric currents flowing in the sea water in horizontal loops, constrained by the resistive land masses of Australia and New Zealand.

7. Discussion

In Section 4 it was established that at both seafloor and land sites, statistically significant spectral lines existed at 1.93 and 2.93 cycle·day^{-1} in the magnetic variation data. The presence of the 2.93 cycle·day^{-1} line implied that a tidally-driven

M_2 ionospheric dynamo was operating during the recording period. The results of separations of the L_2 spectral line into parts of ionospheric and oceanic origin in Section 6 suggested that the ionospheric and oceanic dynamos are equally important sources of signal. These results are in contrast to the analyses of seafloor data by LARSEN (1968) and CHAVE and FILLOUX (1984), which concluded that the $L(M_2)$ ionospheric dynamo was weak because the 1.93 cycle·day^{-1} line was absent at the 90% significance level from magnetic observatory data recorded at Tucson (U.S.A.), but present at the 95% level in seafloor data from the Pacific Ocean. In another study of magnetic fluctuations at Tucson, MALIN (1973) found that 764 days of observatory data showed significant spectral lines, up to 1.7 nT in amplitude, in the $L(M_2)$ set.

The question of the strength of the ionospheric $L(M_2)$ dynamo may perhaps be resolved by considering its seasonal and latitudinal dependence. The dynamo is physically complex with a maximum in summer (February or August depending on the hemisphere), and in winter its action is much reduced, and may even fail (STENING and WINCH, 1979). Thus seasonal variation of the ionospheric dynamo may preclude the use, during the winter months, of the transfer function approach described above.

The published literature contains several theoretical calculations of the natural electromagnetic response to tidal motions. LARSEN (1968) using a thin sheet approximation and CHAVE (1983) more generally have estimated the electromagnetic response for a Kelvin wave propagating along a boundary. The separated oceanic components in Fig. 4 have some qualitative features in common with these theoretical results, but more closely resemble the magnetic response calculated (again using a thin sheet approximation) by HEWSON-BROWNE (1973) for a uniform wave propagating along a channel.

The M_2 tide maps of SCHWIDERSKI (1980) for the Tasman Sea indicate that a uniform wave propagating along a channel may be a good approximation for the tide in the Tasman Sea. The consistency of the oceanic component of the separated magnetic variations with the theoretical tide model response gives much support to the transfer function technique of separation.

The transfer function technique may also be applied to separations other than the $L(M_2, 1.93)$ line. For example, it has been applied to separating the S_2 line into a part driven by the S_2 oceanic tide, and a part due to the S_2 magnetic daily variation harmonic (BINDOFF, 1988). Taking the ratio of the S_2 and M_2 ocean-driven magnetic tides to be the same as given in Table 1, the result is obtained that the vertical component of the seafloor S_2 harmonic in the Tasman experiment data may have a contribution from the ocean tides of up to 2 nT in amplitude.

8. Conclusion

It has been demonstrated that the ionospheric dynamo is present as a significant source of signal in the $L_2(M_2, 1.93)$ spectral line at both land and seafloor sites of the Tasman experiment. The oceanic dynamo contributes to the line at all

seafloor sites, and also at some land sites. The transfer function method has allowed the separation of the contributions of the oceanic and ionospheric dynamos, recorded in the magnetic fluctuation data.

The separations show that for the H and D components the contributions of the ionospheric and oceanic dynamos are comparable. For the H and D components the oceanic source contributes at the seafloor sites only. The Z component, which for the present data is essentially entirely of oceanic-dynamo origin, is significant on both land and at seafloor.

We have many people to thank, especially D. E. Winch who pointed out the existence of the modulated M_2 tide lines, A. D. Chave, I. J. Ferguson, P. J. Mulhearn and K. Lambeck for valuable comments and discussion, and M. N. Sloane for assistance with data reduction. The TPSME experiment was conducted under the US/Australia Agreement for Science and Technology and US participation was supported by the National Science Foundation Grants OCE 83-01216 and OCE 83-12339. Ship-time was provided by the Royal Australian Navy ship HMAS *Cook*. N.L.B. is the recipient of an Australian Commonwealth Postgraduate Research Award.

Appendix 1. Numerical Techniques Adopted to Fit Tidal Lines

The procedure adopted to find the best least-squares fit of the specified tidal lines to each observed data series is now described.

1) Each complete time-series was first band-pass filtered using a recursion technique (SHANKS, 1967; SPATHIS, 1983). The filter was a two-pole Butterworth type, with a low-frequency cut-off of 0.333 cycle·day^{-1} and a high-frequency cut-off of 6 cycle·day^{-1}. Zero-phase filtering was ensured by applying the filter to the time series both forwards and backwards in time. The bandpass filter effectively removed low frequency signals, such as long-period variations due to instrument drift, and other "slow" signals of ionospheric and oceanic origin. The filtering was applied prior to averaging the time series, so that aliasing was minimized.

2) The data were then "hourly-averaged" to form a time series $Y(t)$, and fitted to an equation of form

$$Y(t) = \sum_{n=1}^{S} c_n \cos(2\pi\omega_n t - \phi_n),$$

where c_n and ϕ_n are the amplitude and phase at frequency ω_n cycle·day^{-1}. The symbol t marks the time in days since 0000 hr December 1, 1983 UT. Here S is the number of specified tidal lines.

3) Estimates of errors on the parameters of amplitude and phase were made following BRILLINGER (1981, p. 188).

4) A significance test was performed for each fitted line, following LARSEN (1968) and CHAVE and FILLOUX (1984), by calculating the ratio of the variance of each fitted frequency ω_n to the variance of the background spectrum. The

background spectrum variance is estimated from the average variance of the nearest 10 lines ($1/T$ cycle·day^{-1} apart, from a Fourier series expansion of the data as shown in Fig. 3) centred on ω_n. An F-ratio thus determined can be tested for significance at the 90, 95 and 99% confidence level for 2 over 20 degrees of freedom using standard F-distribution tables.

REFERENCES

BINDOFF, N. L., Electromagnetic induction by oceanic sources in the Tasman Sea, Ph. D. Thesis, The Australian National University, Canberra, 1988.

BRILLINGER, D. R., *Time Series: Data Analysis and Theory*, (expanded edition), Holden Day, San Francisco, 1981.

BULLARD, E. C. and R. L. PARKER, Electromagnetic induction in the oceans, in *The Sea*, Vol. 4, Pt. 2, edited by A. E. Maxwell, pp. 695–730, Wiley, New York, 1971.

CHAVE, A. D., On the theory of electromagnetic induction in the earth by ocean currents, *J. Geophys. Res.*, **88**, 3531–3542, 1983.

CHAVE, A. D. and J. H. FILLOUX, Electromagnetic induction fields in the deep ocean off California: Oceanic and ionospheric sources, *Geophys. J. R. astr. Soc.*, 77, 143–171, 1984.

DOODSON, A. T. and H. D. WARBURG, *Admiralty Manual of Tides*, The British Hydrographic Department, London, 1941.

FERGUSON, I. J., The Tasman project of seafloor magnetotelluric exploration, Ph. D. Thesis, The Australian National University, Canberra, 1988.

FILLOUX, J. H., Magnetotelluric soundings over the Northeast Pacific may reveal spatial dependence of depth and conductance of asthenosphere, *Earth Planet. Sci. Lett.*, **46**, 244–252, 1980.

FILLOUX, J. H., Instrumentation and experimental methods for oceanic studies, in *Geomagnetism*, Vol. 1, Pt. 3, edited by J. A. Jacobs, pp. 143–247, Academic Press, London, 1987.

GOUGH, D. I. and J. S. REITZEL, A portable three-component magnetic variometer, *J. Geomag. Geoelectr.*, **19**, 203–215, 1967.

HEWSON-BROWNE, R. C., Magnetic effects of sea tides, *Phys. Earth Planet. Interiors*, **7**, 161–166, 1973.

LARSEN, J. C., Electric and magnetic fields induced by deep sea tides, *Geophys. J. R. astr. Soc.*, **16**, 47–70, 1968.

LILLEY, F. E. M., F. R. BURDEN, G. W. BOYD, and M. N. SLOANE, Performance tests of a set of Gough-Reitzel magnetic variometers, *J. Geomag. Geoelectr.*, **27**, 75–83, 1975.

LILLEY, F. E. M., J. H. FILLOUX, I. J. FERGUSON, N. L. BINDOFF, and P. J. MULHEARN, The Tasman project of seafloor magnetotelluric exploration: Experiment and observations, *Phys. Earth Planet. Interiors*, 1988 (in press).

MALIN, S. R. C., Separation of lunar daily geomagnetic variations into parts of ionospheric and oceanic origin, *Geophys. J. Roy. astr. Soc.*, **21**, 447–455, 1970.

MALIN, S. R. C., Worldwide distribution of geomagnetic tides, *Proc. Roy. Soc. Lond. A*, **274**, 551–594, 1973.

MATSUSHITA, S., Solar quiet and lunar daily variation fields, in *Physics of Geomagnetic Phenomena*, edited by S. Matsushita and W. H. Campbell, Academic Press, New York, 1967.

MELCHIOR, P., *The Tides of the Planet Earth*, Pergamon, Oxford, 1983.

RODEN, R. B., The effect of an ocean on magnetic diurnal variations, *Geophys. J. Roy. astr. Soc.*, **8**, 375–387, 1964.

SCHLAPP, D. M., Lunar geomagnetic tides and the ocean dynamo, *J. Atmos. Terr. Phys.*, **39**, 1453–1457, 1977.

SCHWIDERSKI, E. W., On charting global ocean tides, *Rev. Geophys. Space Phys.*, **18**, 243–268, 1980.

SHANKS, J. L., Recursion filters for digital processing, *Geophysics*, **23**, 33–51, 1967.

SPATHIS, A. T., Design data for digital Butterworth filters in geophysical data processing, *Bull. Aust. Soc. Explor. Geophys.*, **14**, 63–72, 1983.

STENING, R. J. and D. E. WINCH, Seasonal changes in the global lunar geomagnetic variation, *J. Atmos. Terr. Phys.*, **41**, 311–323, 1979.

VOLLAND, H., *Atmospheric Electrodynamics*, Springer-Verlag, Berlin, 1984.

WINCH, D. E., Spherical harmonic analysis of geomagnetic tides, 1964–1965, *Phil. Trans. Roy. Soc. Lond. A*, **303**, 1–104, 1981.

WINCH, D. E. and R. A. CUNNINGHAM, Lunar magnetic tides at Watheroo: Seasonal, elliptic, evectional, variational and nodal components, *J. Geomag. Geoelectr.*, **24**, 381–414, 1972.